# The cold Leidenfrost regime

Philippe Bourrianne, Cunjing Lv, David Quéré

MATERIALS SCIENCE

# The cold Leidenfrost regime

**Philippe Bourrianne*, Cunjing Lv, David Quéré***

**Superhydrophobicity (observed at room temperature) and Leidenfrost phenomenon (observed on very hot solids) are classical examples of nonwetting surfaces. It was found that combining the two effects by heating water-repellent materials leads to a marked yet unexplained decrease of the Leidenfrost temperature of water. We discuss here how heat enhances superhydrophobicity by favoring a "cold Leidenfrost regime" where water adhesion becomes nonmeasurable even at moderate substrate temperature. Heat is found to induce contradictory effects (sticking due to vapor condensation, and lift due to the spreading of vapor patches), which is eventually shown to be controllable by the solid surface texture. The transition to the levitating Leidenfrost regime is observed to be continuous as a function of temperature, contrasting with the transition on common solids.**



## INTRODUCTION

A volatile liquid on a hot solid levitates above its vapor if the substrate temperature $T$ exceeds the so-called Leidenfrost point (*1*). This temperature, often denoted as $T_L$, is on the order of 200°C for water on smooth metals (*2*), a value that remains to be understood (*3*, *4*). Above $T_L$, levitation provides nonadhesiveness, and it makes liquids spectacularly mobile (*4*): Drops in the Leidenfrost state move under the action of tiny forces, which was exploited to generate self-propulsion on asymmetric textures (*5*). In addition, vapor insulates the liquid from its substrate, which triggers a strong reduction of thermal exchanges (*2*). In contrast, if the solid temperature lies between the boiling point $T_b$ and the Leidenfrost point $T_L$, then the liquid experiences nucleate boiling, with marked consequences on both heat transfer and liquid persistence (*3*).

The thermal properties of both liquid (*2*, *3*, *6*) and solid (*6*, *7*) affect the Leidenfrost temperature. However, the combination of liquid and solid is often imposed by applications, which requires ingenious strategies to control $T_L$ and, thus, the conditions where boiling or insulation happens. Roughness at the solid surface was found to deeply affect the Leidenfrost point. On the one hand, hydrophilic texture can increase $T_L$ up to about 450°C, a way to enhance thermal fluxes and evaporative cooling (*8*, *9*). On the other hand, experiments by Vakarelski *et al.* (*10*) recently suggested that hydrophobic texture may stabilize the vapor layer down to the boiling point $T_b$ of water. The latter situation thus generates a "cold Leidenfrost regime" in water where levitation and its thermal and hydrodynamic consequences are extended by about 100°C compared to usual cases (*11*, *12*). This finding is of obvious practical interest, considering the gain in thermal energy needed to trigger levitation, drag reduction of hot solids (*13*, *14*), or augmented drop lifetime (*10*). By scanning $T$ between room temperature and $T_L$, we explore here the characteristics of the cold Leidenfrost regime.

### The Leidenfrost transition

In Fig. 1A, we first compare the conformation of water drops (volume, $\Omega = 4$ μl) placed on hydrophilic (blue frame) or superhydrophobic (red frame) materials brought to temperature $T$. The hydrophilic solid is a bare silicon wafer that water meets with advancing and receding angles $\theta_a = 42 \pm 2°$ and $\theta_r = 16 \pm 2°$. The repellent material is a wafer coated with hydrophobic nanobeads (Glaco coating; see Materials and Methods), which provides $\theta_a = 165 \pm 2°$ and $\theta_r = 160 \pm 2°$. The wettability contrast between both solids is obvious at $T = 20$°C, and it persists up to $T_b = 100$°C. Beyond $T_b$, nucleate boiling occurs on the hydrophilic substrate, as expected, while neither boiling nor apparent change in drop shape is seen on the superhydrophobic material. It is only above the Leidenfrost point on the hydrophilic material ($T_L \approx 210$°C) that both drops become undistinguishable, a consequence of a similar levitation on vapor. Hence, the Leidenfrost transition on repellent materials cannot be evidenced by direct visualization since water switches from a poorly wetting state at ambient temperature to a vapor-levitating state at high temperature with little change in contact angle. In addition, nucleate boiling does not act as an indicator of temperature when the substrate temperature crosses 100°C, which can be seen as a hallmark of hot repellent materials, an effect that can be further exploited to reduce thermal exchanges and avoid massive gas production.

The sharp contrast between the two materials is also obvious when plotting the lifetime $\tau$ of a given volume of water ($\Omega = 20$ μl) as a function of the substrate temperature $T$ (Fig. 1B). Drops are trapped in shallow cavities machined in aluminum blocks, the metal being either bare (hydrophilic, blue) or Glaco coated (superhydrophobic, red). As seen in the figure, the lifetime on the hydrophilic solid sharply decreases from about 2 min at $T = 85$°C to a fraction of a second above $T_b = 100$°C (boiling regime). At larger $T$, $\tau$ markedly increases up to a maximum that defines the Leidenfrost temperature ($T_L \approx 210$°C). Above $T_L$, $\tau$ slowly decreases with $T$, a classical observation in the Leidenfrost regime: Vapor insulates water from its substrate, which prevents boiling and impedes evaporation. On the superhydrophobic material, the behavior is very different below $T_L$. The lifetime is always much larger than the former, and its decay with temperature is slower, both facts arising from the repellency-induced reduction of solid-liquid contact area. Beyond $T_b$, $\tau$ remains high (a few minutes) and it smoothly decreases with $T$ so that the Leidenfrost transition seems to be continuous instead of abrupt. Last, both lifetimes above $T_L$ become comparable, showing that the Leidenfrost regime at high $T$ does not depend on the solid wettability anymore.

The plot in Fig. 1B raises a number of questions. We know that water (weakly) contacts superhydrophobic materials at room temperature, while it levitates at high temperature, so that we still expect a Leidenfrost transition. The absence of nucleate boiling makes

Physique et Mécanique des Milieux Hétérogènes, UMR 7636 du CNRS, ESPCI, PSL Research University, 75005 Paris, France.
*Corresponding author. Email: philippe.bourrianne@gmail.com (P.B.); david.quere@espci.fr (D.Q.)

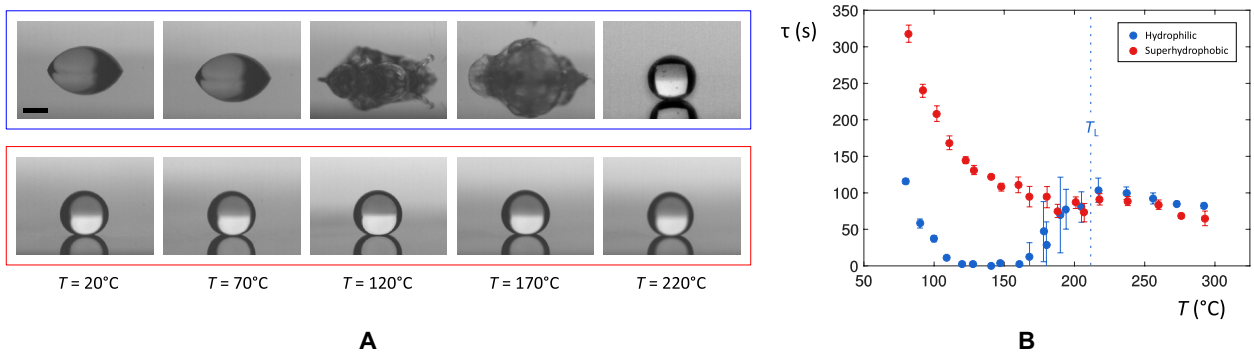


**Fig. 1. Water drops on hot hydrophilic and superhydrophobic materials.** (**A**) Water drops ($\Omega = 4$ μl) on a hydrophilic silicon wafer (blue frame) or on a superhydrophobic Glaco-treated wafer (red frame) brought to temperature $T$. Scale bar, 1 mm. While boiling occurs above 100°C in the hydrophilic case, neither boiling nor apparent change in shape is observed on the repellent solid. Both drops only become similar above 210°C, in a common Leidenfrost state. (**B**) Lifetime $\tau$ of water drops ($\Omega = 20$ μl) as a function of the substrate temperature $T$ on bare aluminum (blue data) and Glaco-treated aluminum (red data). Each point is an average over at least five measurements, and error bars represent standard deviations. The Leidenfrost transition is observed at $T_L \approx 210$°C on the hydrophilic substrate, whereas $\tau(T)$ monotonically decreases in the repellent situation. Beyond $T_L$, both curves superimpose.

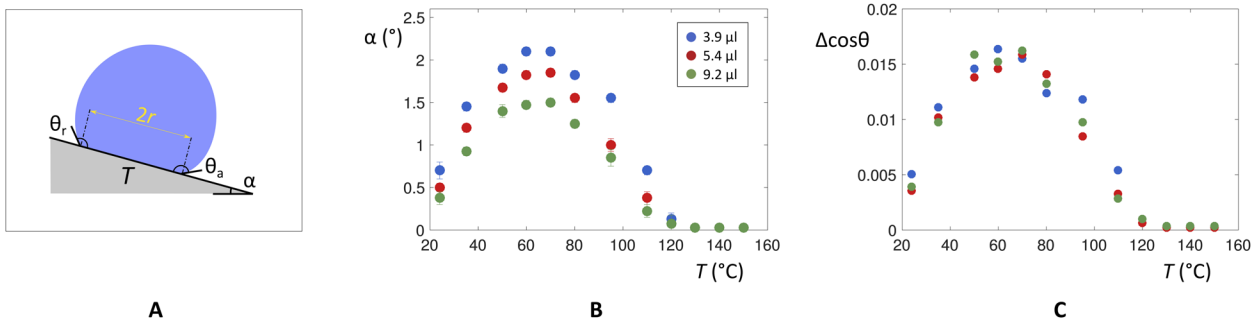


**Fig. 2. Adhesion of water on hot repellent materials.** (**A**) Sketch of the experiment: A water drop with volume $\Omega$ and contact radius $r$ is placed on a substrate brought to a temperature $T$ and tilted until the drop departs. At departure (tilting angle $\alpha$), contact angles at the drop edges are the receding and advancing angles $\theta_r$ and $\theta_a$, respectively. (**B**) Roll-off angle $\alpha$ as a function of temperature $T$ for $\Omega = 3.9$ μl (blue data), $\Omega = 5.4$ μl (red data), and $\Omega = 9.2$ μl (green data). Error bars show the standard deviation for a minimum of five measurements. (**C**) Contact angle hysteresis $\Delta\cos\theta = \cos\theta_r - \cos\theta_a$ deduced from Furmidge's equation: Water adhesion is nonmonotonic as a function of $T$, and it becomes nonmeasurable above ~130°C.

us anticipate a Leidenfrost point $T^* < T_L$, but the continuity in the data does not allow us to detect this point although it makes us suspect that the nature of the transition is modified. Our aim here is to describe what happens on water-repellent substrates below $T_L$, which we do by characterizing the water adhesion and by visualizing the solid-liquid interface.

## Adhesion measurements

Adhesion is classically quantified by the roll-off angle of millimeter-sized drops. We placed a given volume $\Omega$ of water on a Glaco-coated substrate brought to a temperature $T$ and tilted until it reaches the value $\alpha$ at which water departs. As sketched in Fig. 2A, we assume that the drop with apparent contact radius $r$ meets the substrate with respective angles $\theta_a$ and $\theta_r$ at its leading and trailing edges so that the contact angle hysteresis $\Delta\cos\theta = \cos\theta_r - \cos\theta_a$ can be deduced from the force balance at departure, as first discussed by Furmidge (*15*). This balance states $\pi r\gamma(\cos\theta_r - \cos\theta_a) \approx \rho\Omega g\sin\alpha$, denoting $\gamma$ and $\rho$ as the surface tension and density of water and $g$ as the acceleration of gravity. Contact angle hysteresis is a dimensionless measurement of adhesion possibly varying between 0 (no adhesion) and 2 (maximum adhesion).

The critical tilt $\alpha$ is plotted in Fig. 2B as a function of the substrate temperature $T$ for three volumes $\Omega$. Its value logically decreases when drops are larger. The graphs are not monotonic in $T$. The low value of $\alpha$ at $T = 24$°C gradually increases with temperature, and it is multiplied by a factor 3 as the temperature reaches ~70°C, but this regime of enhanced sticking is followed by a decrease in adhesion, up to $T \approx 130$°C, where the critical tilt even becomes nonmeasurable ($\alpha \approx 0$). Hence, Fig. 2B allows us to unambiguously distinguish the small pinning on a water-repellent material (seen at room temperature) from the zero adhesion characterizing a Leidenfrost state. Specifically, the Leidenfrost point is found to be around $T^* \approx 130$°C, a temperature both much smaller than $T_L \approx 210$°C and substantially higher than $T_b \approx 100$°C. By measuring the contact radius $r$ in each experiment (fig. S1) and using Furmidge's equation (where both $\gamma$ and $\rho$ are taken at the substrate temperature $T$), we deduce the contact angle hysteresis $\Delta\cos\theta$. As we plot $\Delta\cos\theta$ as a function of $T$, we observe that the data fairly converge (Fig. 2C): Being a local quantity, $\Delta\cos\theta$ is not expected to depend on the drop volume. Similar results are obtained if the initial drop temperature is the same as that of the substrate (fig. S2) or if experiments are performed with other hydrophobic textures, either colloidal or regularly etched (figs. S3 and S4): Adhesion of water

on a warm superhydrophobic solid generally follows three successive regimes when increasing temperature, which we now discuss.

### The different regimes of adhesion

1) As a substrate gets warmer, water evaporation is favored. The repellent Glaco coating consists of random aggregates of nanobeads forming a porous structure with submicrometric depth, as seen in the image displayed in Fig. 3A. Vapor produced by evaporation can condense inside the pores, which eventually creates liquid bridges between the substrate and the drop (*16*, *17*) and enhances adhesion, as reported in Fig. 2C. We can assess this interpretation by testing a substrate where the formation of these bridges was shown to be negligible. Water condensing on dense arrays of hydrophobic nanocones (Fig. 3B) does not stick on them, a consequence of the geometrical expulsion of water nuclei from conical structures (*17*). Performing the experiment sketched in Fig. 2A allows us to compare adhesion on Glaco coating to that on nanocones with similar adhesion at 20°C (Fig. 3C). Instead of the nonmonotonic behavior reported earlier (blue data), we observe a continuous decay of $\Delta\cos\theta$ from its low value at room temperature to zero above $T^* \approx 130$°C (red data). This experiment thus validates our scenario of condensation-induced adhesion on common water-repellent materials between 20° and 60°/70°C.

2) As seen in Fig. 2C, adhesion decreases from its maximum at ~70°C to its vanishing at ~130°C. Increasing temperature and approaching the boiling point oppose the formation of water nuclei in the texture, which contributes to lower adhesion. We can go further by imaging the bottom interface of the drop. To that end, we use sapphire as a substrate, which combines high thermal conductivity with transparency, the latter property being conserved after Glaco coating owing to the nanosize texture. An inverted microscope (see Materials and Methods) provides an image of the interface at the drop base (Fig. 4A). As shown by Mahadevan and Pomeau (*18*), the radius $r$ of the contact area is expressed by the relationship $r \approx R^2\kappa$, denoting $\kappa^{-1} = (\gamma/\rho g)^{1/2}$ as the capillary length. $\kappa^{-1}$ varies from 2.7 mm at room temperature to 2.5 mm at the boiling point so that the contact radius of a millimeter-size drop is typically 400 μm, significantly smaller than $R$. At moderate temperature ($T < 60$°C), the contact zone is gray with white dots (for $T = 51$°C; Fig. 4B), a heterogeneous appearance arising from air trapped in the texture. This picture is deeply modified above 60° to 70°C. Then, we observe the formation of gray patches with well-defined contours (highlighted in red in the figure for $T = 75$°C). These patches grow as a function of temperature until they fully invade the contact zone where they generate interferences, as seen in Fig. 4B for $T = 150$°C.

The patches are vapor bubbles, as better seen in Fig. 4C, where we display close-up views of their central region. We observe fringes, from which we can deduce that these spherical vapor/liquid interfaces meet the substrate with an advancing contact angle $\theta_v$ as low as 2° (fig. S5): Vapor is close to "wet" the material whose superhydrophobicity implies superaerophilicity. At the same time, the contours of the bubbles are found to be distorted: Vapor bubbles are pinned in the texture and just grow from their nucleation site. Low $\theta_v$ also implies that even a small volume of vapor induces a significant coverage of the solid: A bubble with radius $r_v = 100$ μm encloses a volume $\pi r_v^3\theta_v/4$ of typically 30 pl, which would cover a surface area about 20 times smaller on a smooth hydrophobic surface ($\theta_v = 90$°). The total coverage $\phi_v$ of the surface by vapor can be determined through image analysis. Defined as the ratio of the patch area over the whole contact area $\pi r^2$, $\phi_v$ is, for instance, ~0.4 at 75°C (Fig. 4B). At much larger $T$ (for instance, 150°C in the same figure), $\phi_v$ has reached its maximum $\phi_v = 1$, and the image is fully covered by the fringes arising from the presence of a thin continuous vapor film, as reported on regular (hydrophilic) solids above the Leidenfrost point (*19*, *20*).

We report in Fig. 4D how the vapor coverage $\phi_v$ increases with temperature $T$. We obtained each ensemble of data after depositing a water drop with volume $\Omega = 4$ μl and following the evolution of $\phi_v$ during the first 10 s after deposition (a shorter time compared to the lifetime $\tau$). At fixed temperature $T$, we observed that $\phi_v$ quickly reaches a stationary value that corresponds to the balance between vapor leakage inside the porous texture and vapor injection from the evaporating drop. This stationary value of $\phi_v$ rapidly increases with $T$ around 70°C, a critical behavior that explains the large error bars observed in this regime. Then, it gradually tends toward unity, a behavior accompanied by a decrease of the error bars. The invasion of vapor above 70°C tends to depin water from the solid substrate, which explains the decay of adhesion constituting the second regime in Fig. 2C. The Leidenfrost transition on a superhydrophobic material eventually appears to be a continuous phenomenon, instead of a discontinuous one on regular solids, in agreement with the qualitative observations in Fig. 1.

3) Adhesion becomes nonmeasurable when the Leidenfrost film fully occupies the contact zone, which consistently occurs around

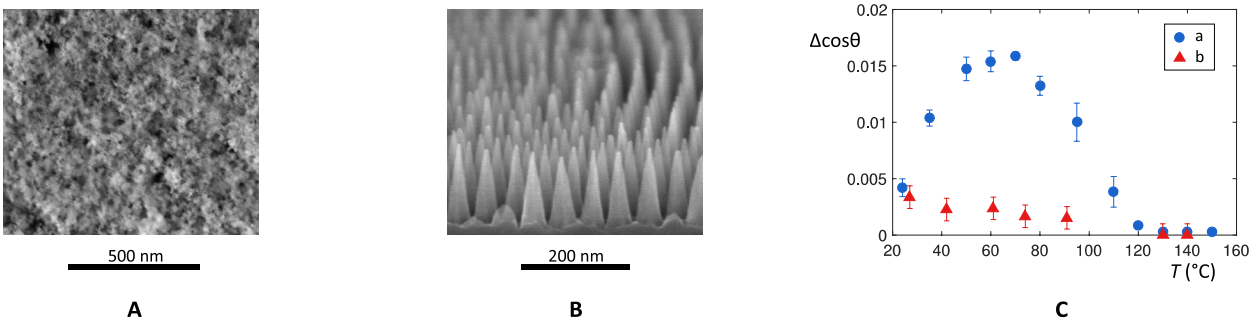


**Fig. 3. Adhesion of water on two kinds of hot hydrophobic nanotexture.** (**A**) SEM (scanning electron microscopy) image of a Glaco-coated brass substrate. Hydrophobic nanobeads deposited on the substrate provide a submicrometric roughness. Scale bar, 500 nm. (**B**) SEM picture of a dense array of nanocones (height, 115 nm; spacing, 52 nm) textured in silicon and coated by fluorosilanes. Scale bar, 200 nm. The picture is adapted from the work of Checco *et al.* (*25*). (**C**) Contact angle hysteresis $\Delta\cos\theta$ of a water drop ($\Omega = 3.9$ μl) on Glaco coating (a, blue data) and on nanocones (b, red data) as a function of the substrate temperature $T$.

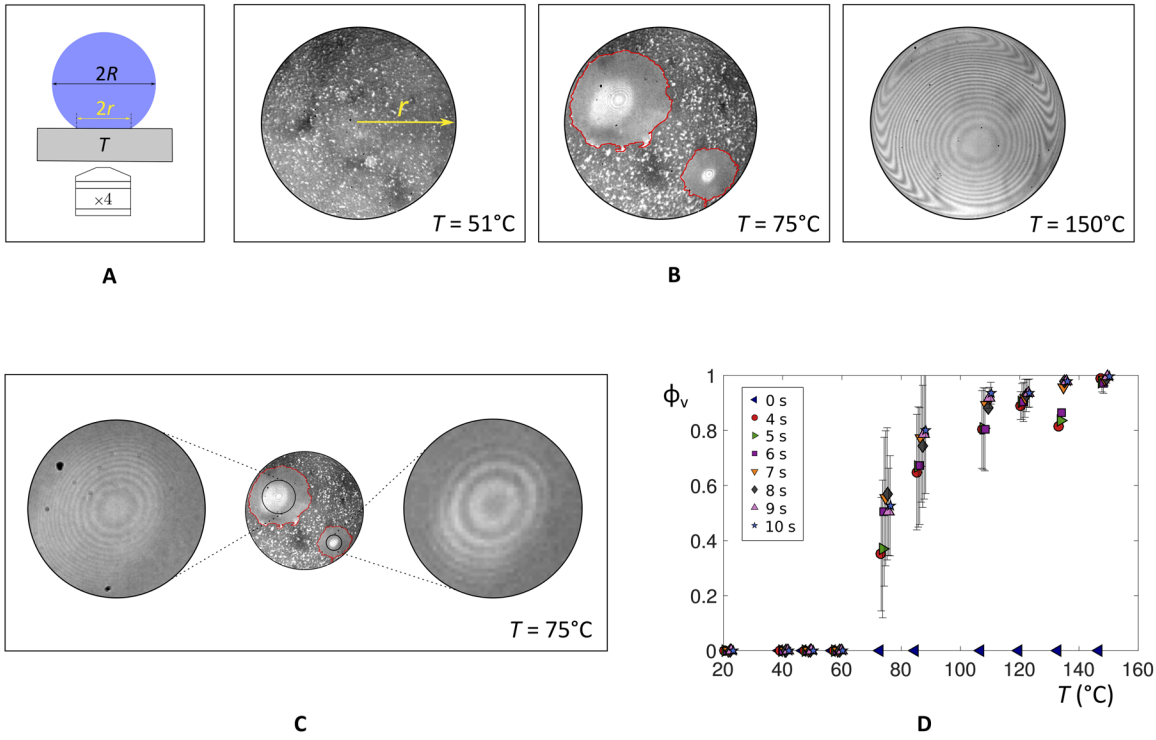


**Fig. 4. Focus on the base of water drops placed on hot repellent substrates.** (**A**) Setup: A drop is deposited on a Glaco-treated sapphire brought to a temperature *T*. The contact zone is observed from below with an inverted microscope. (**B**) Visualization of the contact area whose radius *r* is 0.4 mm for a drop with radius *R* = 1.0 mm at *T* = 51°C (left), *T* = 75°C (center), and *T* = 150°C (right). Vapor patches appear around 70°C, and we highlight their contour in red. (**C**) Close-up on the fringes seen in the central region of the vapor patches seen in (B) at *T* = 75°C. (**D**) Fraction $\phi_v$ occupied by the vapor patches as a function of temperature *T* and measured 0 to 10 s after drop deposition. Each data point is an average over at least three drops, and error bars represent standard deviations. The bars are large in the critical regime of vapor formation and get smaller at larger *T* where they even become negligible when reaching the vapor patch stationary state at large time *t*.

130°C in both Figs. 2C and 4C. Interferences in Fig. 4B show a buoyancy-driven blister, as observed on conventional materials above $T_L$ (*19*–*21*). Apart from an increase in the film thickness, this situation does not evolve when increasing the temperature. Hence, the third regime is an extended Leidenfrost regime, which confirms the observations in Fig. 2C. The Leidenfrost point is lowered by about 80°C compared to flat hydrophilic solids. This strong reduction is made possible by the invasion and coalescence of wetting vapor patches on the highly hydrophobic material, which happens around 130°C. The Leidenfrost transition might naturally occur at the boiling point of water, but this value is slightly shifted in our experiments. The fact that evaporative cooling lowers the solid temperature in the contact zone and that the vapor film insulates the liquid qualitatively explain that the Leidenfrost temperature is larger than 100°C, although the use of hydrophobic texture allows us to approach this limit.

## DISCUSSION

Our interpretation was based on a quasi-static representation of water drops. However, motion is expected in liquids contacting hot solids and thus subjected to temperature differences of a few degrees between their base and their top (*22*). Convection was reported in water evaporating on repellent materials and attributed to both Marangoni and buoyancy effects (*22*, *23*). In fig. S6, we report particle image velocimetry measurements performed in millimetric drops placed on hot substrates. In all cases, we observed a rolling motion at the scale of the drop, with typical velocities *V* in the range of millimeters per second and increasing with the substrate temperature *T*. The viscous force exerted by the drop on the substrate scales as $(\eta V/R)r^2$, and it becomes comparable to the adhesion force $\gamma r\Delta\cos\theta$ when the flow velocity is on the order of $\gamma R\Delta\cos\theta/\eta r$, a speed that can fall to ~10 cm/s for our less adhesive substrates ($\Delta\cos\theta \approx 10^{-3}$). This velocity, however, remains large compared to that measured in the liquid, which justifies why we could neglect the role of these flows in our analysis. Also in the context of dynamics, another case of interest is that of impacting drops. Then, the Leidenfrost transition is known to shift to a (much) higher temperature (*24*) owing to the enhancement of liquid/solid contact brought by inertia. It would be interesting to see how this effect is modified when using repellent materials, a situation where we should observe a weaker Leidenfrost shift than that found with hydrophilic solids.

## MATERIALS AND METHODS

Experiments were carried out using deionized water and various substrates placed on heating plates. The solid temperature was determined using a surface probe with an accuracy of ±1.5°C. The different substrates were silicon wafer, sapphire (from UQG Ltd.), and aluminum or brass samples smoothed with a rubber polishing block supplied by Holmenkol. Tilt angles were measured by a digital inclinometer (accuracy of 0.05°) purchased from RS.

Glaco coating was made with a colloidal solution, the Glaco Mirror Coat Zero purchased from Soft99 Co. Solids drawn out of Glaco solutions are post-baked at 250°C for 30 min, a process repeated three

times to provide a homogeneous coating. After three coatings, the thickness of the coating is submicrometric, as shown by scanning electron microscopy in Fig. 3A. Advancing and receding angles of water at ambient temperature were $\theta_a = 165 \pm 2°$ and $\theta_r = 160 \pm 2°$, respectively, which led to a very low contact angle hysteresis $\Delta\cos\theta$ on the order of $10^{-2}$.

As described by Checco *et al.* (*25*), nanocones are fabricated by combining block copolymer self-assembly with anisotropic plasma etching in silicon, which provides large-area (~4 $cm^2$) textures with ~10-nm feature size and long-range order. Etching is isotropic using a hydrogen bromide:chloride:oxygen ($HBr:Cl_2:O_2$) chemistry, which generates cones with height of 115 nm and spacing of 52 nm. They were made hydrophobic by chemical vapor deposition of 1*H*,1*H*,2*H*,2*H*-perfluorodecyl-trichlorosilane referenced as L16584.03 in VWR.

The base of the drops in Fig. 4 was imaged using a 4× objective mounted on an inverted microscope (AmScope IN300-FL) connected to a high-speed camera (Photron FASTCAM SA3). Illumination was provided via a filter cube (fluorescein isothiocyanate) consisting of a semireflective mirror, a filter ($\lambda = 475 \pm 15$ nm) for the incident light (no filter for the emitted/reflected light).

## SUPPLEMENTARY MATERIALS

Supplementary material for this article is available at http://advances.sciencemag.org/cgi/content/full/5/6/eaaw0304/DC1

Fig. S1. Contact radius *r* of a water drop placed on a hot superhydrophobic solid, as defined in Fig. 2A.

Fig. S2. Contact angle hysteresis $\Delta\cos\theta$ on Glaco-coated substrates as a function of *T* for drops having initially either a temperature $T_d = 20°C$ (blue data) or the same temperature as the substrate ($T_d = T$, red data).

Fig. S3. Water adhesion on heated brass coated by a commercial colloidal repellent material (Ultra-Ever Dry, UltraTech International).

Fig. S4. Water adhesion on heated micrometric posts.

Fig. S5. Morphology of a vapor patch.

Fig. S6. Internal flow in water drops ($R \approx 1.5$ mm) placed on a hot superhydrophobic solid (Glaco-coated wafer).

## REFERENCES AND NOTES


1. J. G. Leidenfrost, *De Aquae Communis Nonnullis Qualitatibus Tractatus* (Ovenius, Duisburg, 1756).
2. B. S. Gottfried, C. J. Lee, K. J. Bell, The Leidenfrost phenomenon: Film boiling of liquid droplets on a flat plate. *Int. J. Heat Mass Transfer* **9**, 1167–1188 (1966).
3. J. D. Bernardin, I. Mudawar, The Leidenfrost point: Experimental study and assessment of existing models. *J. Heat Transfer* **121**, 894–903 (1999).
4. D. Quéré, Leidenfrost dynamics. *Annu. Rev. Fluid Mech.* **45**, 197–215 (2013).
5. H. Linke, B. J. Alemán, L. D. Melling, M. J. Taormina, M. J. Francis, C. C. Dow-Hygelund, V. Narayanan, R. P. Taylor, A. Stout, Self-propelled Leidenfrost droplets. *Phys. Rev. Lett.* **96**, 154502 (2006).
6. K. J. Baumeister, F. F. Simon, Leidenfrost temperature—Its correlation for liquid metals, cryogens, hydrocarbons and water. *J. Heat Transfer* **95**, 166–173 (1973).
7. K. Makino, I. Michiyoshi, The behavior of a water droplet on heated surfaces. *Int. J. Heat Mass Transfer* **27**, 781–791 (1984).
8. C. M. Weickgenannt, Y. Zhang, S. Sinha-Ray, I. V. Roisman, T. Gambaryan-Roisman, C. Tropea, A. L. Yarin, Inverse-Leidenfrost phenomenon on nanofiber mats on hot surfaces. *Phys. Rev. E* **84**, 036310 (2011).
9. C. Kruse, T. Anderson, C. Wilson, C. Zuhlke, D. Alexander, G. Gogos, S. Ndao, Extraordinary shifts of the Leidenfrost temperature from multiscale micro/nanostructured surfaces. *Langmuir* **29**, 9798–9806 (2013).
10. I. U. Vakarelski, N. A. Patankar, J. O. Marston, D. Y. C. Chan, S. T. Thoroddsen, Stabilization of Leidenfrost vapour layer by textured superhydrophobic surfaces. *Nature* **489**, 274–277 (2012).
11. D. A. del Cerro, A. G. Marín, G. R. B. E. Römer, B. Pathiraj, D. Lohse, A. J. Huis in't Veld, Leidenfrost point reduction on micropatterned metallic surfaces. *Langmuir* **28**, 15106–15110 (2012).
12. G. Dupeux, P. Bourrianne, Q. Magdelaine, C. Clanet, D. Quéré, Propulsion on a superhydrophobic ratchet. *Sci. Rep.* **4**, 5280 (2014).
13. I. U. Vakarelski, D. Y. C. Chan, S. T. Thoroddsen, Leidenfrost vapour layer moderation of the drag crisis and trajectories of superhydrophobic and hydrophilic spheres falling in water. *Soft Matter* **10**, 5662–5668 (2014).
14. D. Saranadhi, D. Chen, J. A. Kleingartner, S. Srinivasan, R. E. Cohen, G. H. McKinley, Sustained drag reduction in a turbulent flow using a low-temperature Leidenfrost surface. *Sci. Adv.* **2**, e1600686 (2016).
15. C. G. L. Furmidge, Studies at phase interfaces. I. The sliding of liquid drops on solid surfaces and a theory for spray retention. *J. Colloid Sci.* **17**, 309–324 (1962).
16. Y. Liu, X. Chen, J. H. Xin, Can superhydrophobic surfaces repel hot water? *J. Mater. Chem.* **19**, 5602–5611 (2009).
17. T. Mouterde, G. Lehoucq, S. Xavier, A. Checco, C. T. Black, A. Rahman, T. Midavaine, C. Clanet, D. Quéré, Antifogging abilities of model nanotextures. *Nat. Mater.* **16**, 658–663 (2017).
18. L. Mahadevan, Y. Pomeau, Rolling droplets. *Phys. Fluids* **11**, 2449–2453 (1999).
19. J. C. Burton, A. L. Sharpe, R. C. A. van der Veen, A. Franco, S. R. Nagel, Geometry of the vapor layer under a Leidenfrost drop. *Phys. Rev. Lett.* **109**, 074301 (2012).
20. F. Celestini, G. Kirstetter, Effect of an electric field on a Leidenfrost droplet. *Soft Matter* **8**, 5992–5995 (2012).
21. J. H. Snoeijer, P. Brunet, J. Eggers, Maximum size of drops levitated by an air cushion. *Phys. Rev. E* **79**, 036307 (2009).
22. D. Tam, V. von Arnim, G. H. McKinley, A. E. Hosoi, Marangoni convection in droplets on superhydrophobic surfaces. *J. Fluid Mech.* **624**, 101–123 (2009).
23. S. Dash, A. Chandramohan, J. A. Weibel, S. V. Garimella, Buoyancy-induced on-the-spot mixing in droplets evaporating on nonwetting surfaces. *Phys. Rev. E* **90**, 062407 (2014).
24. M. Shirota, M. A. J. van Limbeek, C. Sun, A. Prosperetti, D. Lohse, Dynamic Leidenfrost effect: Relevant time and length scales. *Phys. Rev. Lett.* **116**, 064501 (2016).
25. A. Checco, A. Rahman, C. T. Black, Robust superhydrophobicity in large-area nanostructured surfaces defined by block-copolymer self assembly. *Adv. Mater.* **26**, 886–891 (2014).


**Acknowledgments:** We thank C. Clanet and T. Mouterde for many useful discussions and C. Black, A. Checco, and A. Rahman for providing the sample shown in Fig. 3 (B and C). **Funding:** This project was partly funded by the French Agence Nationale de la Recherche through the project "ANR Freeflow," within the French Program "Investments for the Future" under reference ANR-10-IDEX-0001-02-PSL. **Author contributions:** D.Q. conceived the project. P.B. and D.Q. designed the project. P.B. and C.L. performed experiments and analyses. P.B. and D.Q. wrote the manuscript with inputs from C.L. **Competing interests:** The authors declare that they have no competing interests. **Data and materials availability:** The data that support the plots within this paper and other findings of this study are available in the main text and in the Supplementary Materials. Additional data related to this paper may be requested from the authors.

Submitted 14 November 2018
Accepted 21 May 2019
Published 28 June 2019
10.1126/sciadv.aaw0304

**Citation:** P. Bourrianne, C. Lv, D. Quéré, The cold Leidenfrost regime. *Sci. Adv.* **5**, eaaw0304 (2019).

Science Advances

# The cold Leidenfrost regime

Philippe Bourrianne, Cunjing Lv and David Quéré

*Sci Adv* **5** (6), eaaw0304.
DOI: 10.1126/sciadv.aaw0304